

The effects of air bubbles on ultrasound velocity measurements

Sandro Longo

Received: 6 April 2005 / Revised: 12 June 2006 / Accepted: 20 June 2006 / Published online: 18 July 2006
© Springer-Verlag 2006

Abstract We report on experiments on the effects of air bubbles on ultrasound velocity measurements in fluids. We used an acoustic Doppler velocimeter system for measuring the three velocity components in a single point and an acoustic Doppler velocimetry profiler system for measuring axial velocity in several points along the beam. The results suggest that both systems essentially measure the velocity of the bubbles, independent of the low air-volume concentration and of bubble radii in the flow field.

1 Introduction

Because of the entrapment or release of air, many natural and technical fluid flows are two-phase flows. In high-speed flows in open channels, air is entrapped by macroturbulence reaching the free surface. Air entrapment occurs at the toe of a hydraulic jump as well as in most breaking waves. Vapour bubbles develop as a result of cavitation.

Because of frequent unlocking, especially at high void concentration, measurements of fluid velocity using laser Doppler velocimetry (LDV) are quite difficult for a two-phase flow. Better results can be obtained using phase Doppler velocimetry (PDV). PDV makes it possible to measure the velocity and the

diameter of round particles and bubbles. PDV requires complex electronics with several photodetectors; multiple detectors are necessary in order to prevent ambiguity in the analysis of the signal or to compensate for variable refraction index of the particles. PDV ultimately requires optical accessibility to the zone of measurement.

Hot film anemometry (HF) is intrusive and suffers from the presence of gas bubbles, which strongly modify the non-linear response of the system. The presence of bubbles near the hot film is clearly detected in the output signal, but the response of the physical system with respect to heat exchange is distorted and difficult to interpret.

Particle image velocimetry (PIV) can be used with good results but with several other limitations, such as the need for a transparent medium and optical accessibility to the measurement zone.

A good candidate for the measurement of two-phase flows is the Doppler ultrasonic technique. It was initially applied to measure velocity in a single volume (acoustic Doppler velocimetry, or ADV) and recently has been applied to obtain velocity measurements at several points along an axis (acoustic Doppler velocity profiler, or ADVP). ADV and ADVP have several advantages over other measurements of fluid velocity. They can be used in optically opaque fluids such as mud and hot fluids such as liquid sodium (Eckert and Gerbeth 2002). ADVP can give information on spatiotemporal velocity, with the data rate virtually independent of seeding concentration [for a description of ADVP techniques, see Takeda (1990, 1999); Lemmin and Rolland (1997)]. The overall errancy of the technique is closely related to the accuracy of set-up and the precision achieved in evaluating the parameters, such as wave celerity.

S. Longo (✉)
Department of Civil Engineering, University of Parma,
Parco Area delle Scienze, 181/A, 43100 Parma, Italy
e-mail: sandro.longo@unipr.it

The limits are essentially a result of the low data rate, which allows only macro-turbulence measurements, and the reduced spatial resolution in respect to LDA or HF.

In some experiments in velocity measurements in spilling breakers and bores (Longo et al. 2001), the influence of entrapped air on measured velocity was readily evident.

The present experiments were intended to generate two-phase flows (water and air bubbles or water and hydrogen bubbles) in a controllable manner and to measure velocity through ADV and ADP. The purpose was to study the effects of the bubbles on the measurements. In Sect. 2, the paper introduces the goal of the experiments. In Sect. 3, the theoretical approach to a pressure wave moving in a two-phase medium is reported, with a short description of ultrasound techniques for measurements of fluid velocity. Section 4 contains a description of the experimental set-up. The results are detailed in Sect. 5. Section 6 reports on measurements (using ADV) of the velocity of rising bubbles. Conclusions are reported in Sect. 7.

2 Scope and objectives

The aim of the present experimental work is to generate information on the influence of air (gas) bubbles on measurements of velocity in flowing fluids using ultrasound techniques based on Doppler. Experimental studies on this topic are scarce (see Nielsen et al. 1999, for ADV performance in bubbly flows) but necessary: ultrasound velocimetry is increasingly being used, not only in two-phase fluid flows, but also in mud with air bubbles and several types of foodstuff.

In order to generate a relatively easy flow field, we used a cylinder that rotates around a vertical axis and is immersed in water. We generated air bubbles by connecting certain devices to an air-pressure pipe, and we produced hydrogen bubbles through electrolysis.

3 Theory

3.1 The effect of bubbles on ultrasounds

In this section, using results from the literature, we shall verify the extent of correction to wave celerity due to air bubbles. In addition, we shall also verify that, within the limits of the present application, the pressure waves are not dispersive. Consequently, a distinction between phase celerity and group celerity is not necessary.

The presence of gas bubbles in a random or pseudo-random array modifies the celerity of the pressure wave, while refraction, diffraction, reflection and absorption take place at the interfaces. In techniques based on ultrasounds, pressure-wave celerity is important because the target position and target velocity are inferred through the knowledge of the wave celerity.

The celerity of the pressure wave depends on the density and compressibility of the fluid. Treating the two-phase medium as an equivalent, single-phase fluid, the complex sound speed is given by

$$c^2 = \frac{1}{\rho K}. \quad (1)$$

Defining ρ_a and ρ_f as the density of the air and water mass, respectively, and K_a and K_f as the compressibility of the air and water, respectively, the density ρ of the mixture is $\rho = v\rho_a + (1 - v)\rho_f$, and its compressibility K is $K = vK_a + (1 - v)K_f$. v is the bubble volume fraction.

Substituting the expression for mass density and compressibility in Eq. 1, the following relationship is obtained:

$$\frac{c_f^2}{c^2} = \left(1 - v + \frac{vK_a}{K_f}\right) \left(1 - v + \frac{v\rho_a}{\rho_f}\right), \quad (2)$$

where $c_f^2 = \frac{1}{\rho_f K_f}$ is the celerity in pure water. This relationship is valid as long as the bubbles are unaffected by pressure waves.

A more complex expression of the wave celerity can be obtained by considering the deformation of the bubbles for a plane incident wave. The compressibility of bubbles vK_a can be expressed as

$$vK_a = \frac{N\Delta V}{\Delta p}, \quad (3)$$

where N is the number of bubbles having radius a for unit volume, and ΔV is the variation in bubble volume due to ultrasound pressure Δp . If $ka \ll 1$, with k the wave number of the pressure wave, pressure acting on a bubble due to an incident wave can be assumed to be uniform. Otherwise, distribution of the pressure can be expressed by

$$\Delta p = \frac{1}{2a} \int_{-a}^a \sqrt{2} p_p e^{i\omega t} e^{ikx} dx = \sqrt{2} p_p e^{i\omega t} \left(\frac{\sin ka}{ka}\right), \quad (4)$$

in which p_p is the root mean square pressure of the incident wave and x is the coordinate in the direction of

propagation of the plane incident wave (Thuraisingham 1998). The corresponding radial deformation of the single bubble is

$$\zeta = \frac{-i4\pi a^2 [\sqrt{2}p_p(\sin ka/\omega ka)] e^{i\omega t}}{R_m + i[\omega m - (s/\omega)]} \tag{5}$$

in which ζ = radial displacement; $m = 4\pi a^3 \rho_f$ (effective mass riding with the bubble); $i = \sqrt{-1}$; $s = m\omega_R^2$ (stiffness constant of the bubble, with ω_R the resonance frequency of the bubble); and $R_m = \delta\omega m$ is the mechanical resistance, with δ the damping constant given by $\delta = \delta_r + \delta_t + \delta_v$. δ_r , δ_t , and δ_v are the components due to re-radiation, thermal conductivity and shear viscosity.

For bubbles of uniform radius a , Eq. 5 reduces to

$$vK_a = \frac{N(4\pi a^2)^2}{m\omega^2 [(-1 + \omega_R^2/\omega^2) + iR_m/\omega m]} \tag{6}$$

(Thuraisingham 1998).

Hence, on using Eq. 6, Eq. 2 reduces to

$$\frac{c_f^2}{c^2} = (1 - v)^2 + v \frac{\rho_a(1 - v)}{\rho_f} + \left(1 - v + \frac{v\rho_a}{\rho_f}\right) \frac{\lambda^2 Na [(-1 + \omega_R^2/\omega^2) - i\delta]}{\pi [(-1 + \omega_R^2/\omega^2)^2 + \delta^2]} \tag{7}$$

Only the last term in Eq. 7 depends on frequency. It is also assumed that the bubble volume fraction is low enough ($v < 0.1$) to allow bubble interactions to be avoided.

If the wave frequency is much higher than the resonance frequency of the bubbles, the damping constant reduces to re-radiation: $\delta \approx \delta_r = ka$. In the present experiments, this is the case. In fact, the resonance frequency of a single bubble can be evaluated as

$$\omega_R = \frac{1}{2\pi} \left(\frac{3P_{go}}{\rho_f a_0^2} - \frac{2\sigma}{\rho_f a_0^3} \right)^{1/2}, \tag{8}$$

in which σ = surface tension, $P_{go} = P_f - P_v + 2\sigma/a_0$, P_f = absolute fluid pressure, P_v = vapour tension and a_0 = undisturbed bubble radius (see Cheeke 2002).

In the present experiments, the bubble radius is in millimetres. Using Eq. 8, we can easily verify that the corresponding resonance frequency is a few kilohertz, much lower than the frequency of the carrier in both devices (1–10 MHz). This is also true for the small bubbles generated by electrolysis.

A second mechanism of resonance is related to the coherent oscillation of bubbles in a collective mode (Kolaini 1998). It has, however, a frequency of resonance much smaller than the frequency resonance of a single bubble. As a consequence we can confidently assume that $\delta \approx ka$ and, with the further condition $\rho_a < \rho_f$, Eq. 7 reduces to

$$\frac{c_f^2}{c^2} \approx 1 - 2v - \frac{3}{2\pi} \left(\frac{\lambda}{a}\right) \frac{v}{1 + k^2 a^2} \left(\frac{1}{2\pi a} + i\right). \tag{9}$$

If $k^2 a^2 \geq 1$ and $v \ll 1$, Eq. 9 simplifies to

$$c \rightarrow \frac{c_f}{\sqrt{1 - 2v}}. \tag{10}$$

All these expressions can be modified by introducing the bubble radii distribution for non-uniform bubbles.

ADVP was used with a probe at 1 MHz, while ADV has a carrier at 10 MHz; the corresponding wavelength in water is ~ 1.5 mm and ~ 0.15 mm, respectively, while in our experiments $v < 0.05$. Having satisfied all the conditions reported above, we can evaluate the ultrasound celerity using expression 10. The ultrasound celerity has a variation equal to $\sim 5\%$ compared to celerity in pure water. This variation is negligible because in most practical situations wave celerity is subject to stronger variations as a result of fluctuations in temperature or the presence of suspended particles.

3.2 Ultrasound Doppler velocimetry and measuring instruments

Our tests were carried out using two kinds of instruments based on the Doppler effect. The first is an ADVP. The instrument was originally developed for the detection, quantification and evaluation of blood flow. In an ADVP, a piezoelectric probe emits the pulse, and the echoes are detected by the same probe (monostatic configuration). By measuring the time between the emission and reception of the pulse, the position of the target is ascertained, once the ultrasound celerity is known. If one measures the shift in frequency, the target velocity component along the probe axis is detected. The volume of measurement depends on the characteristic of the probe. Because of the lateral spreading of the pressure wave, the volume of measurement increases far from the probe. We used a 1 MHz probe with a diameter of 14 mm and a total angle of divergence of $\sim 15^\circ$. ADVP allows measurements more or less at the same time in several “points” (gates) in the axial location.

The second instrument was an ADV. The principles behind the ADV are the same as those behind the ADVP. The main difference between the two devices is that while the ADVP evaluates the velocity component along the axis probe at several points at a similar time with only a small delay, the ADV evaluates the three components of fluid velocity at a single point, elaborating the echoes as detected by spatially oriented receivers (minimum three). The volume of measurement for the probe used is a cylinder 3–9 mm in length and 6 mm in diameter, starting at 5 cm from the probe. The frequency of the carrier is 10 MHz.

4 Experimental set-up and measurement techniques

The experiments were carried out in a 2.5-m long, 1.0-m wide and 50-cm deep tank. The tank had glass walls and a Plexiglas bottom.

The flow-field generator is a cylinder made of aluminium (Fig. 1). Its diameter is 122 mm and its height 62 mm. It is rotated by an electric motor with variable rotation rates electronically controlled in the range 0–2,000 rpm. For the present experiments, only two relatively low but stable velocities have been used: velocity 1 (~ 170 rpm) and velocity 2 (~ 280 rpm), corresponding to ~ 110 cm/s and ~ 180 cm/s at the outer radius of the cylinder.

4.1 Flow facility

The theoretical approximate flow field can be computed by solving the Navier–Stokes equation for an infinite cylinder rotating in an infinite domain. A sketch of the reference system is presented in Fig. 2. Let us consider the steady-state solutions of the form

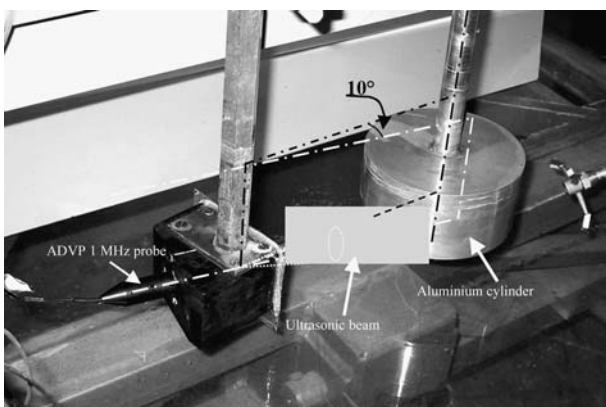


Fig. 1 Experimental set-up

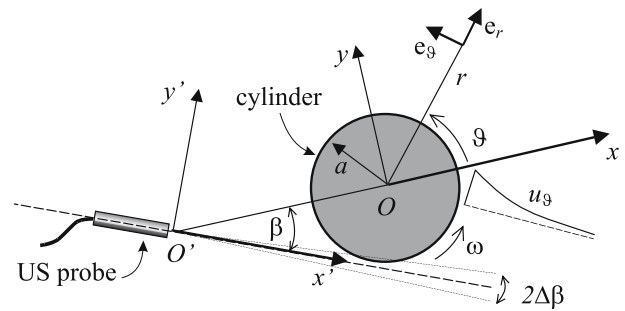


Fig. 2 Coordinate systems for computing the flow field around the cylinder and the velocity component along the ultrasound probe axis

$$u = u_{\vartheta}(r)e_{\vartheta}, \tag{11}$$

with consequent circular streamlines and with the following no-slip boundary condition at the outer radius of the cylinder:

$$u_{\vartheta}(a) = \omega a. \tag{12}$$

Equation 12 automatically satisfies the mass-balance equation. It can be demonstrated that a solution is

$$u_{\vartheta}(r) = \frac{\omega a^2}{r}, \quad \Gamma(r) = 2\pi\omega a^2, \quad r \geq a. \tag{13}$$

In the entire fluid domain, the velocity (only tangential component) radial decays and the circulation is uniform. Our cylinder is immersed in a square tank, and the boundary condition at the walls of the tank is not strictly satisfied by solution 13. A boundary layer also develops at the walls of the tank, where the no-slip condition has to be satisfied.

The velocity component along the US probe axis can be obtained by applying a coordinate transformation to solution 13. It is equal to

$$u_{x'}(x') = \frac{\omega a^2 d \sin \beta}{(x' \cos \beta - d)^2 + (x' \sin \beta)^2}, \tag{14}$$

where $d = |\overline{OO'}|$ and x' is the distance along the US probe axis.

By including the effects of the US field dispersion, the measured velocity can be obtained averaging over the two extremes $\beta_1 = \beta - \Delta \beta$ and $\beta_2 = \beta + \Delta \beta$, obtaining

$$\overline{u_{x'}}(x') = \frac{\omega a^2}{2x'(\beta_2 - \beta_1)} \ln \left(\frac{d^2 - 2x'd \cos \beta_2 + x'^2}{d^2 - 2x'd \cos \beta_1 + x'^2} \right). \tag{15}$$

According to Eq. 15, measured velocity should monotonically increase from the tip of the probe, with a maximum near the surface of the cylinder.

Near the outer radius of the cylinder, the boundary effect on ultrasounds reduces the S/N ratio significantly. Near the tip of the probe, the boundary layer damps the velocity to 0.

The discrepancies between the theoretical laminar profiles and the measured profiles are caused by (1) the growth of instabilities, (2) three-dimensional phenomena owing to the finite length of the cylinder, (3) tank boundaries (bottom and free surface) and (4) the spreading of turbulence. This enhances the transfer of momentum, even though it is expected that far from the cylinder, turbulence and velocity decay.

4.2 Bubbly flow generators

We tested some devices in order to obtain bubbly flow with a bubble volume fraction of up to 5% and bubble diameters between a few hundred micrometres and a few millimetres. The best results were obtained using commercial oxygenators in balsa wood, as used for aquaria. The oxygenators used are parallelepipeds $6 \times 6 \times 2 \text{ cm}^3$ with an air-supply tube 6 mm in diameter. The air is forced into the tank through the wood fibres, which are uniformly packed. The radius and void concentration of the bubbles generated depend on the air pressure. Each oxygenator was connected separately to an air supply through a pressure-valve reducer with a micrometry regulator. The average air pressure in the supply pipe is $2.5 \times 10^5 \text{ Pa}$, and it is reduced to $\sim 5 \text{ kPa}$ by the pressure reducer. Unfortunately, the device was unable to generate high-volume concentration flows because the higher pressure generated unstable and non-uniform bubbles, and it was used only for tests with void concentration $< 1.55\%$. A second device was built. It is a PVC pipe with a diameter of 140 mm connected through a pipefitting to a PVC pipe with a diameter of 80 mm (Fig. 3). The air is insufflated in a chamber, which is separated by the water through a balsa wood separator 3 cm thick, with the fibre plane parallel to the tube axis.

The initial air flux is 140 mm in diameter and is then reduced to 80 mm, increasing the air-volume concentration about threefold. This device was called the “chimney”, the analogy being obvious.

The bubble-volume fraction was measured using an impedance probe (Ma et al. 1991; Lamarre 1993). Impedance probes are based on the difference in electrical conductivity and dielectric constants between liquid and vapour or gas and are suitable for averaged

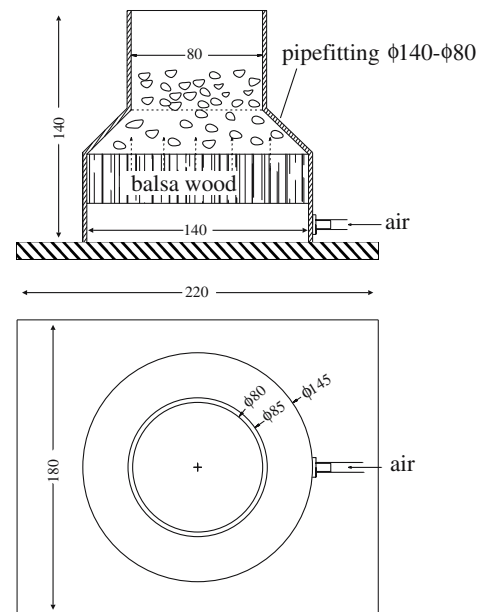


Fig. 3 Device for generating high air-volume concentration (“chimney”)

volume fraction measurements. Our probe has two electrodes made of nickel–chromium wires whose diameter is 0.3 mm connected to a 4 kHz oscillator. The wires are fixed by PVC fittings. The output signal of the impedance probe is filtered with a low-pass filter at 4 Hz and acquired by a PC through an A/D board.

The output of the probe depends on geometry, and it was necessary to calibrate it. The calibration was performed in a cylindrical bubble tank with air insufflated in a chamber at the bottom and diffused through a balsa wood diffuser. Owing to the presence of air bubbles, the bulk density of the mixture drops and the free surface level rises. Measuring the absolute pressure at the level of the static taps allows for the evaluation of the average mass density and hence of the average air-bubble volume fraction. Several geometries of probes were tested (Corradi 2002). The calibration curve for the probe we adopted is a third-order polynomial (Fig. 4).

The geometric characteristics of the bubbles were measured using photographs taken with a digital camera. Several pictures were taken, contouring the bubbles having sharp contours (in the focus plane). Most bubbles appear as ellipsoids. We defined the equivalent volumetric radius

$$a_{\text{vol,eq.}} = \sqrt[3]{3}(a_{\text{max}})^2 a_{\text{min}} \quad (16)$$

as the radius of a sphere having the same volume as an ellipsoid with the axis orthogonal to the focal plane equal to $2a_{\text{max}}$; a_{max} and a_{min} are the maximum and

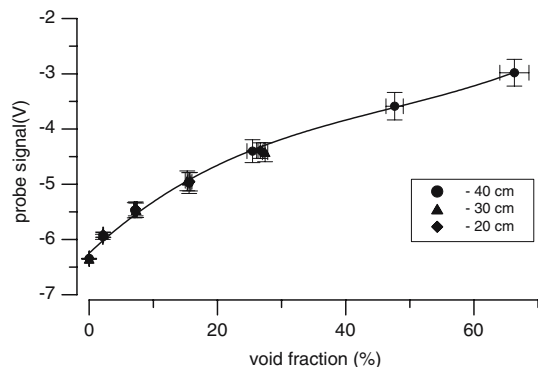


Fig. 4 Void-fraction probe calibration. First probe. Bubbly flow homogeneity test

minimum semi-axis of the ellipses, as observed in the photo. The shape parameter is the ratio a_{\max}/a_{\min} . In Fig. 5, two histograms typical of bubble production are shown.

4.3 Single bubbles generator

In order to generate single bubbles and a very low void concentration (and small radius), we used an insulin needle (27 G, 0.4 mm external diameter) with careful control of the air-supply pressure (Fig. 6).

The measured bubble radius is 0.76 ± 0.3 mm, and the emission rate is nearly 50 bubbles per second.

4.4 Hydrogen bubbles generator

The last device was a hydrogen bubble generator based on electrolysis. The electrolysis device had the two electrodes made of nickel–chromium wires with a diameter of 0.3 mm connected to a DC 24 V source, with electric-flow current in the test condition equal to 0.24 A. The radius of the hydrogen bubbles was not measured, but it is assumed in the range 10–100 μm (Volanshi et al. 1996). The bubble-volume fraction is extremely low and cannot be detected and

Fig. 5 Histograms of bubble production, 0.6 ± 0.3 mm (test 1 in Table 1). Number of bubbles ≈ 570

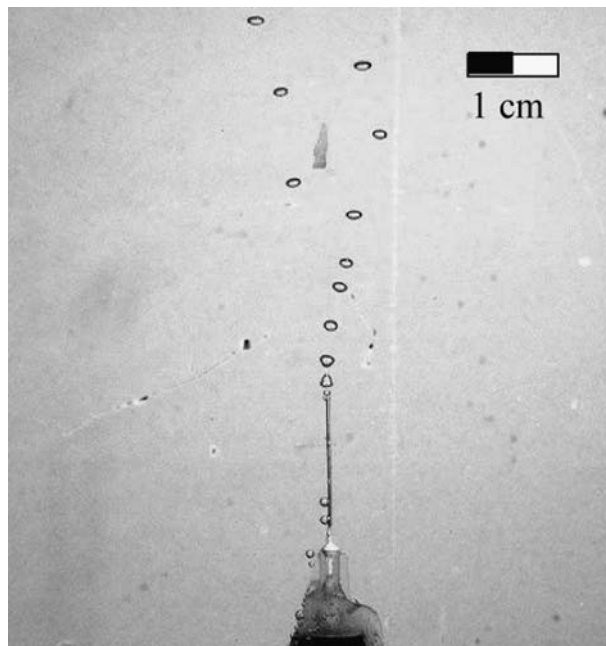
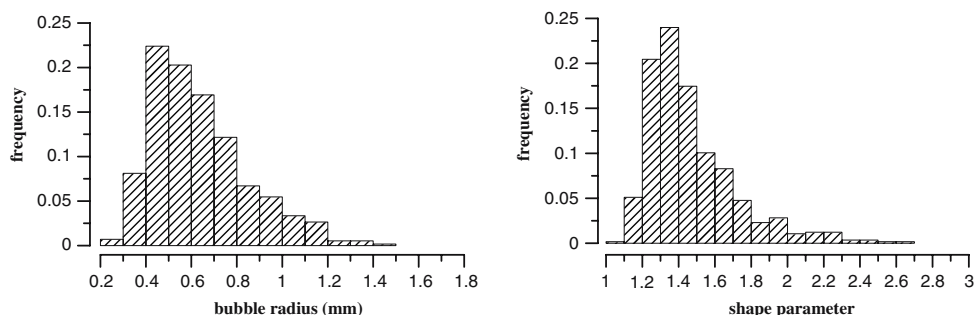


Fig. 6 Train of bubbles generated by the insulin needle. Digital camera, f 8.0-1/1000s

measured by the impedance probe, but a crude estimate is possible. The gas discharge is computed on the basis of the electric current. For our device, the discharge of hydrogen under standard conditions is equal to 7×10^{-7} m^3/s , the area of generation is $\sim 190 \times 10^{-4}$ m^2 , and the mean velocity for $v = 1$ (only gas) should be $\cong 3.7 \times 10^{-5}$ m/s. The actual rising velocity of the hydrogen bubbles is of the order of 1 cm/s, giving a bubble volume fraction of $\sim 3.7 \times 10^{-3}$.

Different bubbly flow regimes are observed as the void concentration and the bubble size is increased:

- At low void concentration and small bubble radius, the bubbles rise in a stable and regular way. They do not collapse or coalesce.
- At high void fraction concentration, the bubbles are unstable and the bubbly flow pulsates.

- The micro-bubbles generated by electrolysis tend to diffuse and reach a very low rising velocity.

5 Description of the tests

5.1 Measurements using the ADVP

All tests were carried out with the rotation rate of the cylinder set at the two lower values of ~ 170 rpm and ~ 280 rpm. The corresponding peripheral velocities are ~ 110 cm/s and ~ 180 cm/s. The probe of the ADVP is in the plane of rotation, with the axis forming an angle of incidence of ~ 10° with the normal to lateral surface (see Fig. 1). Test conditions are summarized in Table 1.

Data were collected averaging 512 emissions per profile with spatial resolution (intended as the distance between the baricenter of two subsequent volumes of measurement measured along the probe axis) equal to 2.2 mm. Each emission consisted of a burst containing eight cycles with a size of the volume of measurements equal to 6 mm. The probe tip was at ~ 10 cm from the surface of the cylinder. The first recording point was at 15.7 mm from the tip of the probe (to avoid the disturbed near field); the last point was at 101 mm. The data rate was ~ 8 Hz (frequency of acquisition and elaboration of 512 profiles). The number of profiles acquired for post-processing was 5,000, corresponding to ~ 600 s. Some preliminary measurements were carried out in still water for checking the Doppler noise level of the ADVP. The results were negligible.

The computed mean velocity profiles are reported in Fig. 7, and the velocity standard deviation (STD) profiles are shown in Fig. 8. One of the measurements lasted for 20,000 profiles, in order to test the stability of the process.

The data in Figs. 7 and 8 clearly document the strong influence of air bubbles on measured velocity. The STD of velocity is always higher in bubbly flows

Table 1 Test conditions (measurements with the ADVP)

Test no.	Void concentration v (%)	Bubble radius (mm)	Shape parameter	Generator
1	0.13 ± 0.05	0.6 ± 0.30	1.47	Small generators
2	0.53 ± 0.1	1.3 ± 0.36	1.86	
3	1.55 ± 0.15	1.7 ± 0.41	1.94	
4	0.59 ± 0.1	1.4 ± 0.37	2.03	Chimney
5	2.03 ± 0.2	1.8 ± 0.42	2.18	
6	5.35 ± 0.2	2.3 ± 0.45	2.03	

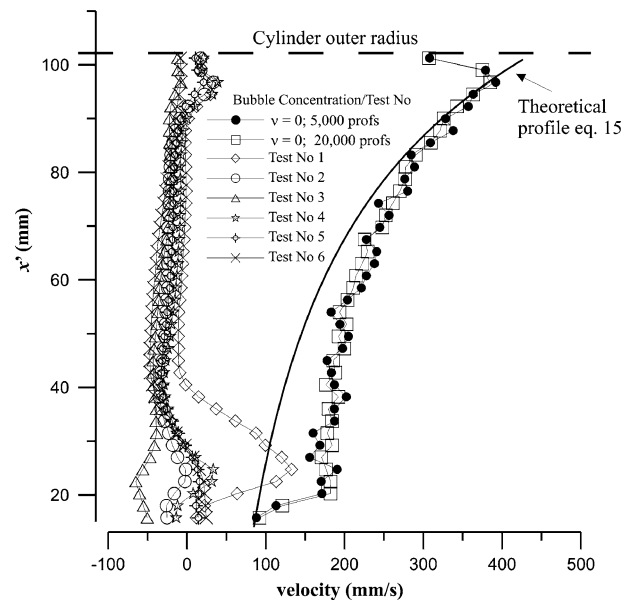


Fig. 7 Mean velocity profiles, first set of tests with the ADVP

than in pure water. It is not caused by turbulence enhancement only, and the presence-absence sequences of bubbles plays a major role in signal fluctuations. Similar results were obtained by increasing the emitted energy and the gain, checking also the energy of the echoes.

In addition to the test conditions in Table 1, three hydrogen bubble fluxes were introduced in the flow field, taking up all the space between the probe and the cylinder (test 1, not reported), part of the space nearest to the cylinder and part of the space nearest to the probe (test numbers 2 and 3 in Fig. 9). The probe tip

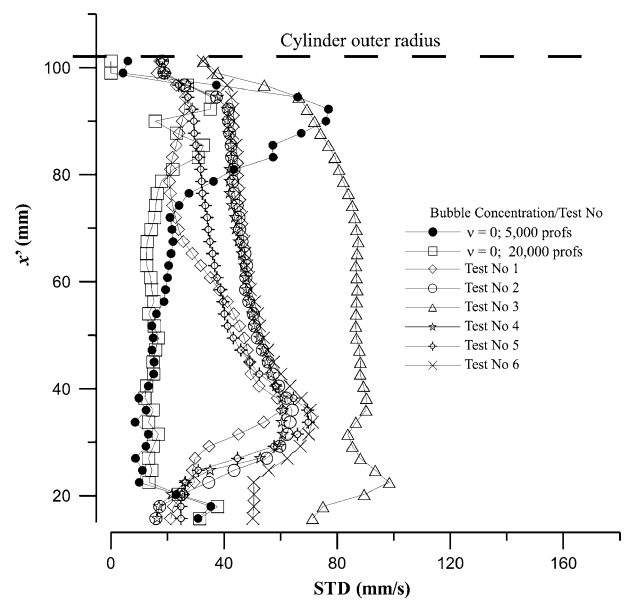


Fig. 8 STD velocity profiles, first set of tests with the ADVP

was at ~ 14 cm from the cylinder surface with a spatial resolution (US beam axis) of 3 mm.

Occasionally, some spurious data appear in the profile. Observing the profiles, the first impression is that the instrument is able to measure the bubble velocity instead of the fluid velocity or a phasic average velocity. The flow field generated by the cylinder is unable either to accelerate the bubbles significantly or to cause their path to deviate from the vertical. As a consequence, the measured flow fields have to be correlated to the bubble plume dynamics. The importance of micro-bubbles in US signal scattering has already been highlighted in case of high frequency US. Experimental results by Shen and Lemmin (1997, 2000) indicate that micro-bubbles able to follow the turbulent motion of fluid elements allow for the resolution of flow turbulence. In the present tests, the bubbles do not follow the flow field, but the signal scattered by the micro-bubbles overcomes in intensity the signal scattered by the tracer particles and by other sources of echoes in the flow field. They also induce a bias of the peak frequency towards the velocity of the bubbles.

5.2 Measurements using the ADV

The ADV probe was set up in order to have the measurement volume near the outer radius of the rotating cylinder (Fig. 10). The x -component is in the

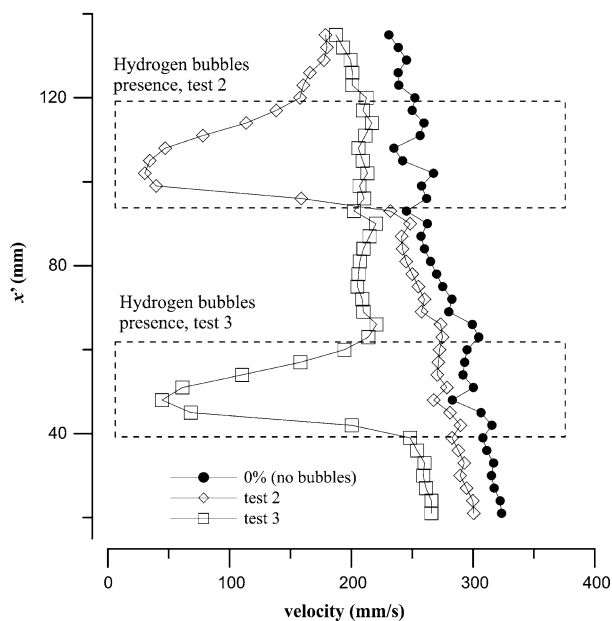


Fig. 9 Mean-velocity profiles with hydrogen bubbles present only in the part of the domain between the cylinder and the probe

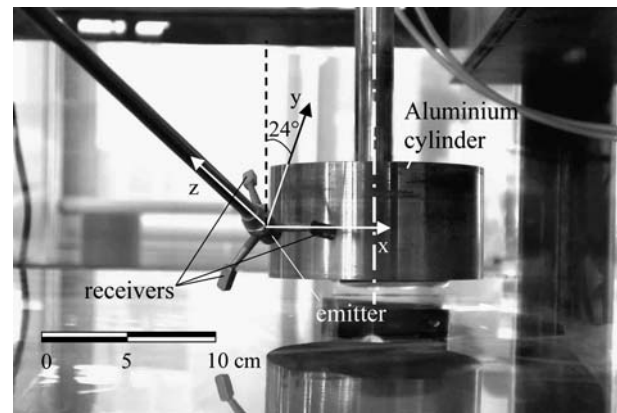


Fig. 10 Set-up of the ADV probe

horizontal plane and should be equal to the peripheral velocity of the cylinder. The y -component is at $\sim 24^\circ$ to the vertical. The z -component is orthogonal to the x and y components.

Two sets of experiments were carried out, with six bubble characteristics and two rotation rates of the cylinder. Data were acquired for 300 s and then elaborated, extracting some classical statistical parameters. The results reveal behaviour similar to that of the ADVP. The V_x component is strongly damped, whereas the V_y component increases with increasing bubble radius. The z -component always has negligible values.

The void concentration of bubbles is very low. The results seem to show that the measured velocity is bubble velocity and not fluid or phasic (weighted) average velocity. In order to check this behaviour, a new configuration has been tested. The bubbles are generated below the cylinder, with the axis of the vertical plume nearly coincident with the axis of rotation of the cylinder. As soon as the bubbles reach the lower surface of the cylinder, they are radial-accelerated and detach from the cylinder with a horizontal component of velocity close to the peripheral velocity of the cylinder. It is more evident with small bubbles than bigger bubbles. After detaching, buoyancy accelerates the bubbles in the vertical direction and drag reduces the velocity component in the horizontal plane.

Tests were carried out with two rotation rates of the cylinder. For comparison, bubbles were generated below the cylinder (strong entrapment by the fluid flow, progressively reduced due to detachment from the boundary layer of the lateral surface) and near the lateral surface of the cylinder (reduced entrapment by the fluid flow) (Table 2).

Table 2 Test conditions (measurements with the ADV)

ADV no. 1	ADV no. 2	ADV no. 3	ADV no. 4
170 rpm (110 cm/s)	170 rpm (110 cm/s)	280 rpm (280 cm/s)	290 rpm (280 cm/s)
Below the cylinder	Near the lateral surf	Below the cylinder	Near the lateral surf

Results for V_x and V_y are shown in Figs. 11 and 12. Because of the orientation of the probe, the velocity component V_y represents the bubble rising velocity by $\cos 24^\circ$. The error bars represent $\pm 15\%$ the estimated velocity (Bowles and Daffern 1997).

Note that the vertical velocity for bubbles generated below the cylinder (empty symbols in Fig. 12) tend to be negative, presumably as a consequence of stable macrovortices.

6 Bubble-rise velocity using the ADV

The experiments herein described indicate that the ADV (and the ADVP) essentially measures bubble velocity. In order to compare our results with the results of other authors, a set of experiments was set up with various bubble plumes in still water. Measurements of terminal bubble-rise velocity are compared with similar experiments by Haberman and Morton (1954), also cited in Kobus (1991).

Bubble-rise velocity has various expressions according to the regime (Kobus 1991):

- For small bubbles (spherical regime) the bubble-rise velocity is

$$v_b(\text{m/s}) = 1.448a^2(\text{mm}) \quad (a) \quad (17)$$

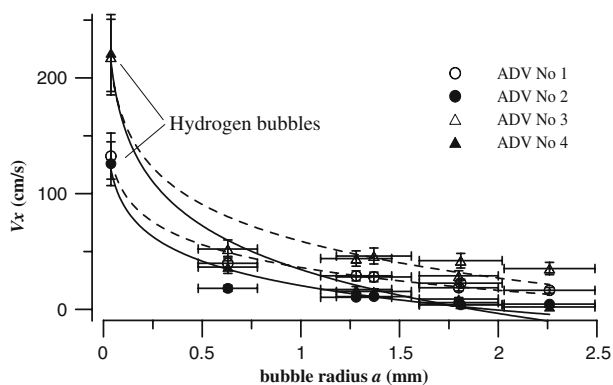


Fig. 11 Horizontal velocity component V_x versus bubble radius. Filled symbols (filled circle, filled triangle) refer to bubbles generated laterally with respect to the cylinder. Empty symbols (open circle, open triangle) refer to bubbles generated below the cylinder

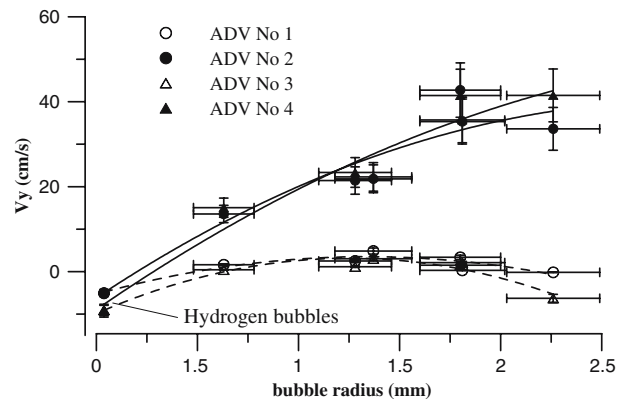


Fig. 12 Measured velocity V_y versus bubble radius. For caption, see Fig. 11

- For bubbles having a diameter in the range 0.2–20 mm, the rise motion is unstable and spiral motion can occur. The results are different for pure and contaminated water. The velocity is in the range 0.1–0.4 m/s, and the regime is ellipsoidal.
- For large bubbles of a spherical cap shape, the results are

$$v_b(\text{m/s}) = 0.1a^{1/2}(\text{mm}) \quad (a > 10 \text{ mm}). \quad (18)$$

The results are summarised in Fig. 13 and compared to results in Haberman and Morton (1954). The measured V_x components are negligible, and the ratio V_z/V_y is equal to $\tan(24^\circ)$ (~ 0.44), decomposing the bubble-rising velocity along x and z , as expected.

Bubble-rising velocities measured by the ADV are generally higher than experimental velocities reported in Haberman and Morton (1954), valid for a single

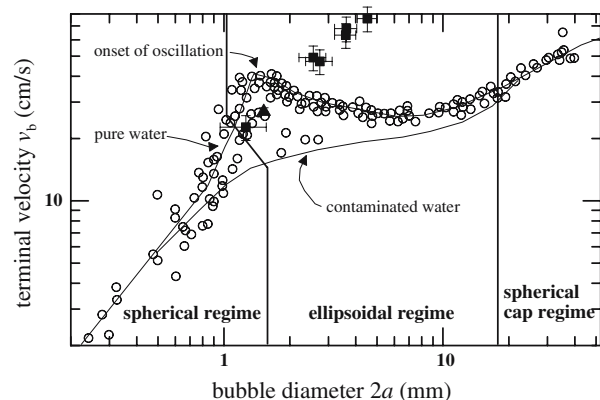


Fig. 13 Bubble-rising velocity of a single air bubble in an extended body of water at rest. Open circles refer to Haberman and Morton (1954). Squares refer to present experiments with the generation of multiple bubbles (see Table 1). The triangle refers to sequential bubbles generated by an insulin needle

bubble. It is consistent with the experimental evidence that the bubble swarm in an unconfined flow induces an upward flow of water, with effective rising velocities two or three times higher than those for a single bubble. In a confined flow, mass balance requires a downward flow of water, which reduces the bubble-rise velocity. In the present experimental set-up, the bubble plume is small in relation to the size of the tank and can confidently be assumed as being unconfined.

7 Conclusions

The conclusions essentially refer to the range 1–10 MHz of the ultrasound carrier and are strictly limited to the range of void fraction of the present experiments.

- Experiments and analysis of the results show that measurements of velocity using ultrasound Doppler-based velocimeters in a two-phase flow field (air or hydrogen bubbles and water) give the velocity of the bubbles. This is because bubbles scatter sonic energy efficiently and, in a detection algorithm based on spectral peak estimation of the echoes, they unavoidably dominate the scenario.
- This effect is independent of the void bubble volume fraction and still applies to micrometry hydrogen bubbles.
- In most practical situations (bubble volume fraction < 0.1) and using a carrier with a frequency far from the resonance of the bubbles, ultrasound celerity is unaffected by the presence of bubbles, and the celerity in pure water can be adopted with negligible error. Thermal stratification usually has a more important effect on the wave celerity of ultrasound.
- Because of the nature of bubbly flows, the STD of the measured velocity is relatively high and is not a good indicator of turbulence energy. Frequent velocity spikes owing to the presence or absence of bubbles increase the data dispersion without a correlation to turbulence.

Acknowledgments This study was supported by FIL2004. Many thanks to Michele Corradi, who immensely helped in carrying out the experiments during his master's thesis. Many thanks also to the reviewers for their valuable suggestions.

References

- Bowles CB, Daffern CD (1997) The independent calibration of the acoustic Doppler velocimeter. In: XXVII IAHR International Congress
- Cheeke JDN (2002) Fundamentals and applications of ultrasonic waves. CRC Series in Pure and Applied Physics, CRC Press LLC, pp x+462, ISBN 0849301300
- Corradi M (2002) Effetti delle bolle d'aria sulla misura di velocità di un fluido con strumenti ad Ultrasuoni. Master's Thesis, University of Parma, p 189 (in Italian)
- Eckert S, Gerbeth G (2002) Velocity measurements in liquid sodium by means of ultrasound Doppler velocimetry. *Exp Fluids* 32(5):542–546
- Haberman WL, Morton RK (1954) An experimental study of bubbles moving in liquids. In: *Proc ASCE* vol. 80 pp 379–427
- Kobus HR (1991) Introduction to air–water flows. In: Air entrainment in free-surface flows, Wood IR (ed) *Hydraulic structures design manual* (1991) vol. 4, IAHR Monography, Balkema, Rotterdam, ISBN 90 6191 994 0, pp vii+142
- Kolaini AR (1998) Sound radiation by various types of laboratory breaking waves in fresh and salt water. *J Acoust Soc Am* 103:300–308
- Lamarre E (1993) An experimental study of air entrainment by breaking waves. Ph.D. Thesis, MIT, Boston
- Lemmin U, Rolland T (1997) Acoustic velocity profiler for laboratory and field studies. *J Hydr Eng* 1089–1097
- Longo S, Losada IJ, Petti M, Pasotti N, Lara JL (2001) Measurements of breaking waves and bores through a USD velocity profiler. Technical Report UPR/UCa_01_2001, University of Parma, E.T.S.I.C.C. y P., Ocean & Coastal Research Group Laboratory, Universidad de Cantabria, Spain
- Ma Y, Chung N, Pei B, Lin W, Hsu Y (1991) Two simplified methods to determine void fractions for two-phase flow. *Heat Transf Fluid Flow* 94:124–133
- Nielsen KD, Weber LJ, Muste M (1999) Capabilities and limits for ADV measurements in bubbly flows. XXVIII IAHR Congress, Graz
- Shen C, Lemmin U (1997) Ultrasonic scattering in highly turbulent clear water flow. *Ultrasonics* 35:57–64
- Shen C, Lemmin U (2000) Intensity fluctuations of ultrasonic scattering in a highly turbulent flow. *Ultrasonics* 37:603–613
- Takeda Y (1990) Development of ultrasound velocity profile monitor. *Nucl Eng Design* 126:277–285
- Takeda Y (1999) Ultrasonic Doppler method or velocity profile measurement in fluid dynamics and fluid engineering. *Exp Fluids* 26:177–178
- Thuraisingham RA (1998) Sound speed in bubbly water at megahertz frequencies. *Ultrasonics* 36:767–773
- Volanshi A, Olthuis W, Bergeveld P (1996) Gas bubbles electrologically generated at microcavity electrodes used for the measurement of the dynamic surface tension in liquids. *Sensor Actuat A* 52:18–22